

The effect of vehicle velocity and drift angle on through-body AUV tunnel thruster performance

Aaron Saunders¹ and Meyer Nahon*²

¹*Boston Dynamics, Waltham MA 02451, USA*

²*Mechanical Engineering, McGill University, Montreal, Canada, H3A 2K6*

(Received July 29, 2011, Revised December 8, 2011, Accepted December 9, 2011)

Abstract. New applications of streamlined Autonomous Underwater Vehicles require an AUV capable of completing missions with both high-speed straight-line runs and slow maneuvers or station keeping tasks. At low, or zero, forward speeds, the AUV's control surfaces become ineffective. To improve an AUV's low speed maneuverability, while maintaining a low drag profile, through-body tunnel thrusters have become a popular addition to modern AUV systems. The effect of forward vehicle motion and sideslip on these types of thrusters is not well understood. In order to characterize these effects and to adapt existing tunnel thruster models to include them, an experimental system was constructed. This system includes a transverse tunnel thruster mounted in a streamlined AUV. A 6-axis load cell mounted internally was used to measure the thrust directly. The AUV was mounted in Memorial University of Newfoundland's tow tank, and several tests were run to characterize the effect of vehicle motion on the transient and steady state thruster performance. Finally, a thruster model was modified to include these effects.

Keywords: autonomous underwater vehicles; AUV thrusters; through-body thrusters; tunnel thrusters; thruster modeling.

1. Introduction

Streamlined AUVs have traditionally been used in high-speed missions that require the vehicle to cover large distances or long missions that require high endurance. Tasks that involve precision positioning, have in most cases, been beyond the capabilities of these AUVs. Such missions generally make use of bluff bodied cage-style Remotely Operated Vehicles (ROV) which are much more maneuverable by virtue of their multiple thrusters mounted on the perimeter of the vehicle. Unfortunately this configuration dramatically increases the overall drag of the vehicle.

Streamlined AUVs generally use hydrodynamic control surfaces to steer the vehicle. These control surfaces lose their effectiveness at low speeds. In order to provide increased maneuverability at low speeds without changing the low drag profile of the AUV, through-body thrusters, also known as tunnel thrusters, can be added. Adding tunnel thrusters enables the vehicle to travel long distances at high speeds to a desired destination and then perform tasks that require station keeping such as environmental inspection. This effectively merges the maneuverability strengths of ROVs with the hydrodynamic efficiency of AUVs. Several AUVs such as the NPS ARIES (Marco and Healy

*Corresponding author, Professor, E-mail: Meyer.Nahon@mcgill.ca

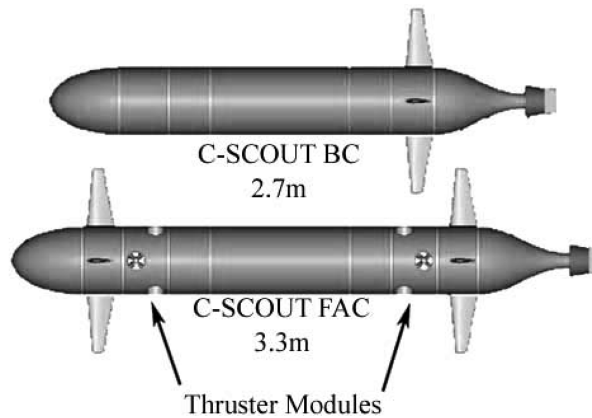


Fig. 1 Top view of C-SCOUT configurations; BC-base configuration, FAC- fully actuated configuration

2000), C-SCOUT (Curtis *et al.* 2000), and REDERMOR (Mailfert and LeMaire 1998) make use of tunnel thrusters for low speed maneuverability.

The C-SCOUT (Canadian Self-Contained Off-the-shelf Underwater Testbed) AUV (Curtis *et al.* 2000) was designed to be able to cruise ahead or astern with a high degree of maneuverability, and to hover, even in a cross-current. As shown in Fig. 1, it is streamlined in shape, and has control planes for control while underway, and through-body tunnel thrusters for hover and low speed control. The baseline configuration (BC) of the vehicle has four control surfaces aft, and a single thruster aft for propulsion. The fully-actuated configuration (FAC) has the four aft control surfaces, but also four control surfaces toward the front of the vehicle. In addition, the fully actuated version is equipped with six through-body thrusters: two thrusters are to be placed vertically; one forward and one aft, and the remaining four are to be placed horizontally two forward and two aft. The tunnel thruster placements give low-speed control in pitch, heave, yaw, roll, and sway, with surge control accomplished by the main propulsor.

The basic concept of through-body tunnel thrusters in AUVs is very similar to that of bow-thrusters used to maneuver large ships. It is therefore appropriate to mention the literature relating to bow thrusters, some of which dates back to the 1950's. These works deal primarily with steady-state bow thruster performance. For example, Beveridge (1972) discusses the hydrodynamic forces and moments produced by bow thrusters, and reports that thruster effectiveness is reduced substantially during forward and astern travel relative to bollard pull conditions.

Yoerger, Cooke and Slotine (1990) showed the importance of including the thruster dynamics when designing underwater vehicle control systems. Several dynamic models have been developed to represent the transient performance of tunnel thrusters using momentum theory with a blade element model for the propeller. A historical summary of recent work in lumped-parameter thruster dynamics modelling is given by Whitcomb and Yoerger (1999). The first work directly related to small AUV tunnel thrusters was done by McLean (1991) at the Naval Postgraduate School on the AUV II tunnel thruster. Brown (1993) and Healey *et al.* (1995) adapted McLean's momentum based model to use the blade element, lift/drag, theory to model the propeller in a tunnel thruster model. Models presented by Bachmayer *et al.* (1998, 2000) later expanded the basic four-quadrant models to include additional fluid effects such as rotations and presented a method for experimentally determining nonsinusoidal lift/drag curves.

An important step in modelling the performance of any physical system is validating the

numerical model. The experiments completed by McLean (1991), Brown (1993), Whitney and Smith (1998) and Bachmayer *et al.* (2000) made use of small tanks or water channels to measure the performance of a stationary thruster. In Brown's (1993) model, four parameters tied to the specific design of the tunnel and propeller were determined empirically by matching the computer simulation with the experimental axial force data. The experimental setup of Whitney and Smith (1998) and Bachmayer *et al.* (2000) used a more sophisticated 6-axis load balance setup for measuring axial thrust and hydrodynamic torque. Those works also used a 3-D Doppler flow meter to measure flow velocities at the thruster intake and outlet, which allowed the estimation of empirically derived lift/drag coefficient curves.

The effect of forward vessel motion was considered in the model presented by Blanke *et al.* (2000). That model was developed similarly to Brown's (1993), but also considers a non-zero ambient water velocity. As well, Kim and Chung (2006) investigated the effects of non-zero and non-parallel ambient flow velocity on the performance of a shrouded thruster. There, a model was also developed showing good correspondence between experimental and simulation results. However, incorporation of a thruster in a through-body arrangement in a vehicle will have substantial impact on the tunnel thruster performance.

Researchers have begun to incorporate through-body thruster models in vehicle simulations to investigate vehicle control and performance. For example, Evans and Nahon (2004) used a simulation to compare the maneuvering performance of the C-SCOUT vehicle, with and without through-body thrusters. As well, Palmer *et al.* (2008) used a simulation with a through-body thruster model to determine the optimum speed at which the Autosub vehicle should transition from survey to low-speed maneuvering modes.

As noted, apart from the work of Kim and Chung (2006), the models mentioned above do not include the effects of forward vehicle motion or vehicle orientation on through-body thruster performance. In order to adapt existing tunnel thruster models to include these effects, an experimental system was built to characterize the effects of forward vehicle speed and drift (sideslip) angle on tunnel thruster performance. This system includes a transverse tunnel thruster mounted in a model of the C-SCOUT AUV and a 6-axis load cell mounted internally to measure thrust. The model was mounted in Memorial University of Newfoundland's tow tank. This paper discusses the experimental setup, the results obtained from tow tank testing, and the incorporation of these results into a computer simulation.

2. Experimental system

2.1 Thruster and controller

Fig. 2 shows the layout of the thruster system. The major components include:

- Personal Computer (PC) running LabVIEW software for the control and data acquisition user interface.
- Keithley PCI Data Acquisition Card (DAC), interface to the Maxon controller
- Maxon servo amplifier/controller
- Thruster Unit: Maxon servomotor, gearbox, propeller
- ATI Force/Torque load cell and ISA controller card to power the load cell and convert the raw sensor data into 6-axis force information.

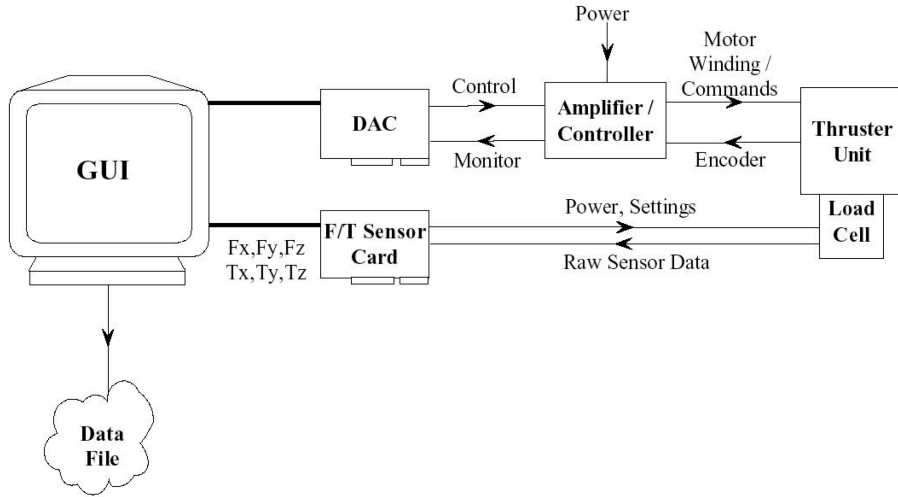


Fig. 2 Thruster system schematic

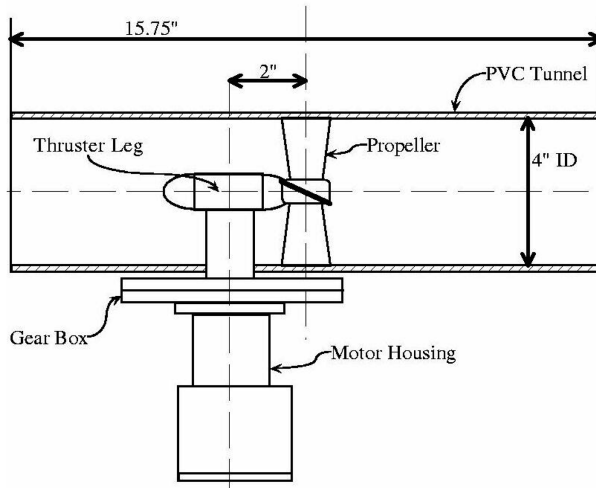


Fig. 3 Tunnel thruster layout

The Maxon motor and controller contain an internal speed sensing and control loop allowing the motor to be driven by commands in rotational speed, rather than by current commands as used by Brown (1993) and Healey *et al.* (1995).

Fig. 3 shows the general layout of the thruster components. The tunnel thruster unit consists of the following major components: Maxon Servomotor, Reduction Gearbox (5:1), Thruster Leg, Propeller, and a 102 mm (4 in) ID PVC Tunnel.

A custom propeller was fabricated due to the difficulties in locating an off-the-shelf propeller for the 102 mm (4 in) tunnel diameter. The propeller is a four blade Kaplan style propeller with unity pitch to diameter ratio; blade area ratio of 0.55; 100 mm (3.95 in) OD; and 24 mm (0.9375 in) hub diameter.

In order to test the tunnel thruster in the full scale C-SCOUT, all the thruster components

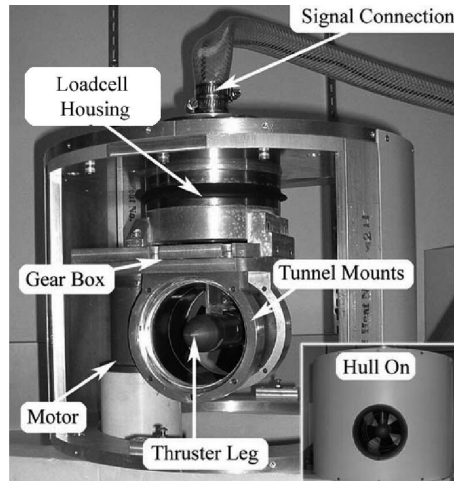


Fig. 4 Thruster module

including the load cell needed to be mounted inside a 305 mm (12 in) long tunnel thruster module. The resulting module is shown in Fig. 4. An ATI Gamma multi-axis force/torque (F/T) sensor was used to measure the required thruster loads. This transducer had ranges of ± 133.4 N (± 30 lb) in F_x and F_y ; ± 445 N (± 100 lb) in F_z ; and ± 11.3 Nm (± 100 in-lb) in all three torque axes.

In the experimental system, a crucial issue in mounting the thruster unit (which includes all the labeled components in the main part of Fig. 4) into the module is ensuring the mechanical isolation of the thruster unit from the module (or hull). Because the load cell measures the forces generated by the entire thruster unit, any contact between the hull and tunnel entrances would result in incorrect load information. The tunnel entrances were designed to match the hull shape and be offset by 1.6 mm (1/16 in). The design of the intakes was not optimized---they simply match the hull curvature and have 22 mm (7/8 in) rounded edges. The lack of a faired inlet into the tunnel implies that vortices could form at the tunnel entry when the thruster is operated while the AUV has significant forward speed. The load cell will measure any forces/moments generated by the propeller itself, as well as hydrodynamic forces acting on the inside of the tunnel and on the thruster leg. It will not measure hydrodynamic forces acting on the external faces of the module or remainder of the hull. As such, the load cell will not measure secondary effects that operation of the thruster may have in modifying the hull hydrodynamics.

The module was bolted directly into a model of the C-SCOUT AUV, and the entire model was mounted to a yaw assembly and mounted on the tow tank carriage. The AUV model used for these experiments was a full scale replica of the C-SCOUT vehicle. This model was built to enable research on the hydrodynamic properties of the C-SCOUT and various types of propulsion systems currently being developed.

2.2 Tow tank

Fig. 5 shows the configuration of the C-SCOUT model as mounted on the tow carriage. The model was moved through the water at various constant drift angles and speeds in the MUN tow tank in order to quantify the effects of vehicle speed and orientation on thruster performance. The tow tank is 54.7 m long (~ 32.2 m usable), 4.57 m wide with an adjustable water depth up to 2.5 m

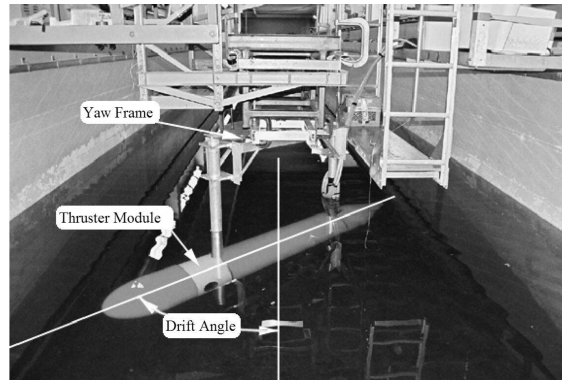


Fig. 5 Tow tank

and a top carriage speed of 5.0 m/s. The C-SCOUT model had to be held below the water and set at various drift angles. To do this, a Yaw Frame was designed to mount to the tow carriage load points and hold the two struts on the C-SCOUT model, as shown in Fig. 5. The lower half of the yaw frame could be rotated and fixed through $\pm 90^\circ$ of rotation in 5° increments.

3. Experimental results

3.1 Test procedure

The testing in this work focussed on a single tunnel thruster module mounted in one location on the vehicle. It is expected that hull interaction will play a large role in the experimental results. Testing one location on the vehicle will only provide information for that location and the data obtained may not be applicable to other thruster locations. In addition, the results may be vehicle dependent and therefore may not be directly applicable to other vehicles. A test procedure was developed to ensure that the desired information would be captured in the test results. The C-SCOUT vehicle was designed to have a top speed of 4 m/s. The operational range of the vehicle investigated in this work can be split into three regimes:

- Maneuvering/hovering, in cross currents up to 0.5 m/s
- Forward Travel - zero drift angle forward travel
- High Speed Turning with side-slip

It was important to create a test matrix to cover all three regimes of operation. It was also important to obtain both steady state and transient test data for each regime. By testing drift angles between $\pm 90^\circ$ at speeds up to 0.5 m/s the entire Maneuvering range is satisfied. Testing up to 4 m/s at zero drift angles covers the Forward Travel condition. The last regime is the high speed turns with side-slip. The yaw frame was not designed to hold the vehicle against large hydrodynamic loads experienced during large drift angles and high carriage speeds. It was therefore necessary to minimize the range of angles tested at higher speeds. It was estimated that, during C-SCOUT operation, a maximum-rudder turn at a vehicle speed of 1.5 m/s would result in a side-slip angle of 20° . The High Speed Turning range was therefore selected to include this point. A pictorial representation of the resulting test matrix can be seen in Fig. 6. In total, there are 86 test cases for each the steady state and transient tests.

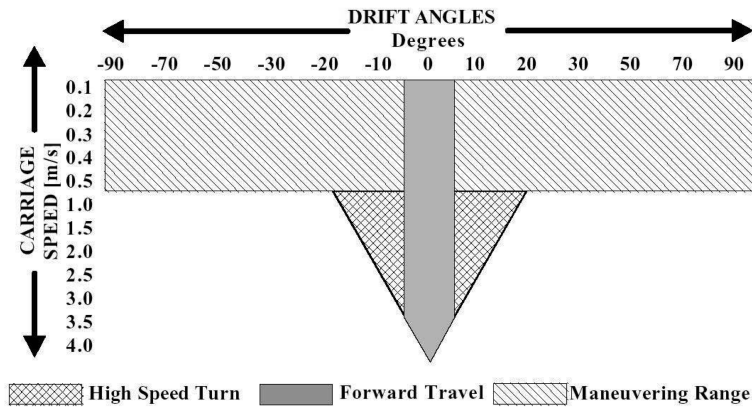


Fig. 6 Test matrix

3.2 Steady-state results

Prior works have shown that a thruster’s steady state thrust is proportional to the square of the propeller RPM (Yoerger *et al.* 1990, Bachmayer *et al.* 2000, Healey *et al.* 1995, Whitcomb and Yoerger 1999, Whitney and Smith 1998). This was verified in the present work, as shown in Fig. 7. However, it was noted that the constant of proportionality (slope of Fig. 7) is 26.7% higher for reverse RPM than for forward RPM. This forward/reverse asymmetry is not uncommon, and must be accounted for when modeling the thruster behaviour.

For the steady state tests in the tow tank, the thruster unit was always operated in a positive rotational direction, which results in water flow from left to right in Figs. 3 and 8(a). When oriented at +90° drift angle, Fig. 8(c), the oncoming water is coming in the same direction as the thruster tries to drive it. Kim and Chung (2006) denoted this the ‘equi-directional state’ in their work. In

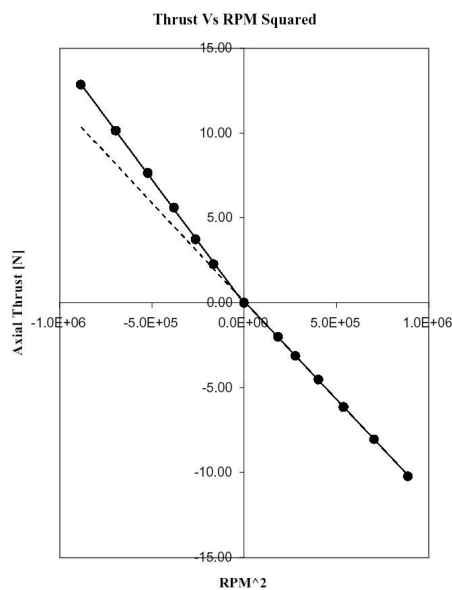


Fig. 7 Steady-state static thrust results

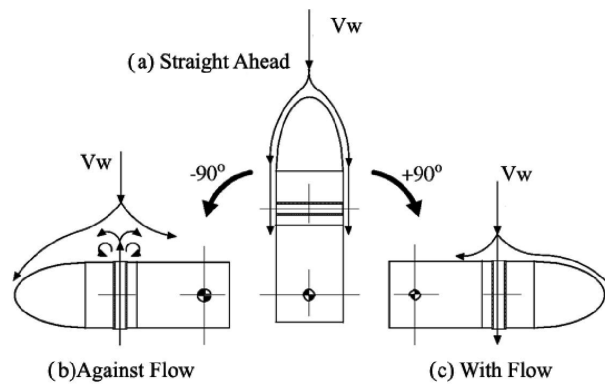


Fig. 8 Flow cases

Fig. 8(b), at -90° , the opposite occurs: the water exiting the thruster is being pushed into the oncoming water, denoted as the ‘anti-directional state’ by Kim and Chng (2006). It is expected that these complicated flow conditions will have a large effect on the thruster performance. The only important assumption made before starting the tests is that the asymmetry in the thrust will remain the same as in the static tests. This allows us to use the slope difference for the stationary tests (Fig. 7) to convert the positive rotation propeller data into negative rotation.

It would take a very long time to complete an individual test matrix for several steady-state propeller speeds. In order to reduce test time, the motor speed was slowly ramped from zero to full speed for each constant carriage speed and drift angle from the test matrix. Several values on the ramp were compared to true steady state thrust and the values matched closely. It was therefore assumed that the data from the slow ramp, was an accurate representation of the steady state performance.

Axial thrust is again plotted against propeller RPM squared. Fig. 9 shows two sample plots (for $V = 0.4$ m/s, Drift = $\pm 50^\circ$) from the test matrix. The linear relationship between axial thrust and RPM squared still appears to hold when the vehicle is moving forward with drift. However, it is apparent from Fig. 9 that the y -intercept is no longer zero but varies with orientation and carriage speed. In the ‘anti-directional state’, represented by the case where Drift = -50° , a ‘thrust force’ exists even at zero RPM, presumably because the flow entering the tunnel exerts pressure on the stationary propeller. In the ‘equi-directional state’, represented by the case where Drift = $+50^\circ$, a corresponding force is generated in the opposite direction, for the same reason. It is interesting to note that the thruster’s ability to generate thrust by increasing RPM seems reduced in the anti-directional state relative to the equi-directional state (i.e., the slope is less in the former case).

The relationship between steady state thrust and RPM squared implied by Fig. 9 is

$$F_a = a + b\omega_p|\omega_p| \quad (1)$$

where F_a is the axial thrust, a is the y -intercept in [N], b is the slope in [N/RPM²], and ω_p is propeller speed in [RPM].

The fact that all the steady state experimental data follows the relationship given by Eq. (1) indicates that we can study these results simply by looking at how a and b vary with vehicle speed and drift angle. For each test case, the slope and y -intercept were extracted, and the results are

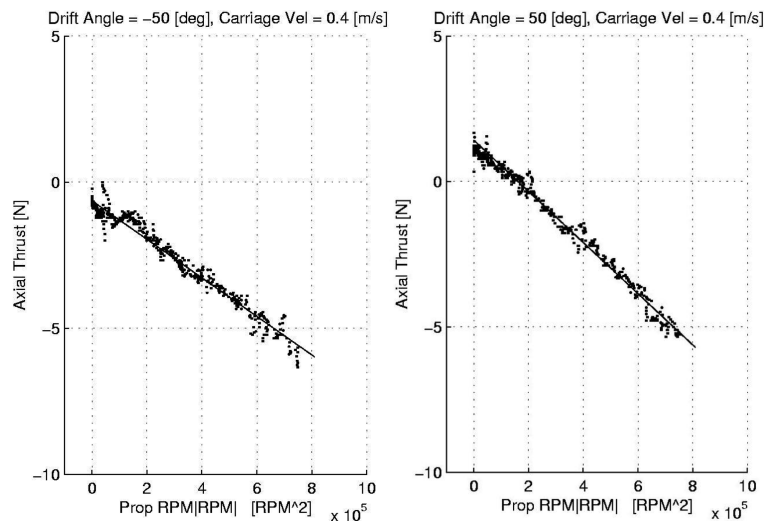


Fig. 9 Thrust at $V = 0.4$ m/s, Drift = -50° and Drift = $+50^\circ$

plotted in Fig. 10 for test cases in the Maneuvering range.

Maneuvering: The Maneuvering range contains the bulk of the experimental tests. In general, axial thrust performance is reduced slightly as carriage speed is increased, as shown in the lower part of Fig. 10. At low speeds, the slope values do not change much as a function of drift angle. As carriage speed is increased, the magnitude of the slope falls more quickly with speed. For drift angles between -50° and -70° there is a dramatic drop in axial thrust performance, to about half the low speed value. This is thought to be caused by the fluid interaction at the thruster outlet and the disturbance to the inlet caused by the body of the vehicle. This is not of great concern, considering that a negative drift angle and a positive propeller speed correspond to the thruster trying to move the vehicle in the same general direction as the oncoming flow---not a likely occurrence in a station-keeping or hovering operation.

The behavior of the y -intercept is relatively intuitive: as the component of the oncoming speed along the thruster's longitudinal axis increases (increasing speed, increasing drift angle), the load cell senses a force in that same direction. When the drift angle is negative, the y -intercept is also negative and increases in magnitude with increasing speed. Between $\pm 30^\circ$, the intercept curves do not appear to be affected much by carriage speed. At larger drift angles and higher speeds, the intercept becomes more significant.

The complexity of the curves in Fig. 10 suggest that there is no simple relationship between vehicle speed, drift angle and axial thrust. It is likely that the complex fluid dynamical effects of hull interaction have a large effect on thruster performance. As a result, the performance characteristics of the tunnel thruster cannot be de-coupled from the C-SCOUT model, making the data vehicle dependent.

Forward Travel: The intercept and slope data for the high speed tests at zero drift angle are shown in Fig. 11, and further details of this data can be found in Saunders (2002). Because the vehicle is completely symmetrical about its longitudinal plane, the pressure at the tunnel intake and exit should be the same, resulting in zero net flow through the tunnel at zero RPM. Therefore, the y -intercept a should remain zero for the full range of speeds. The intercept values are very close to zero at low speeds but then become significant beyond 1.0 m/s, and appear to increase quadratically

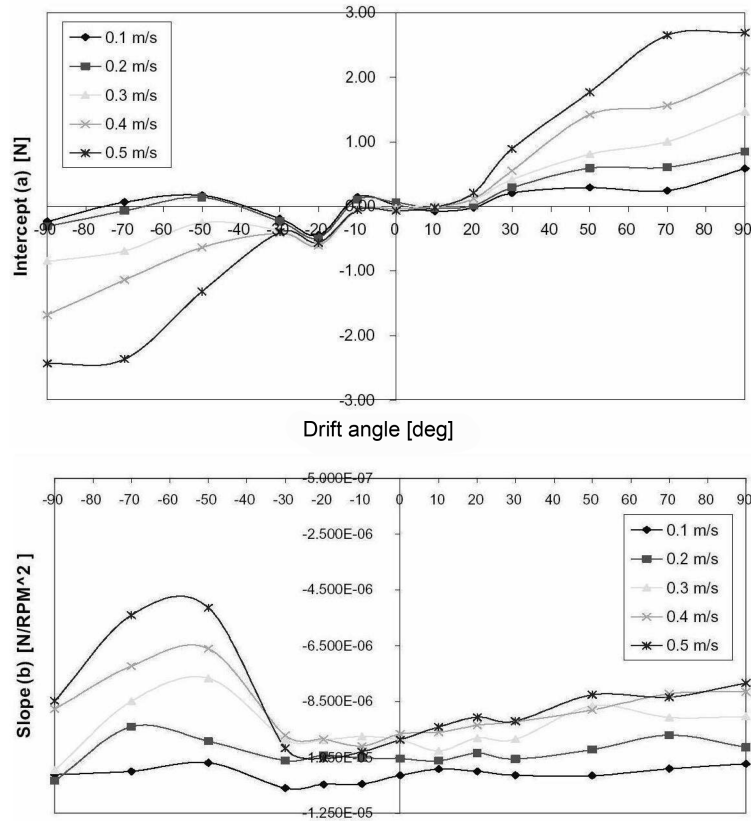


Fig. 10 Maneuvering range axial thrust intercept and slope values

with carriage speed (reaching 3.5 N at 4 m/s). It is suspected that a misalignment of the vehicle model with respect to the direction of travel of the tow carriage caused this to occur. Based on the fact that the plots of a versus drift angle crossed zero at the same location (-7°) for all values of carriage speed, it would appear that the model was misaligned by that angle. At the time of the tests, a series of indirect measurements was relied upon to align the vehicle, but a misalignment of 7 between the vehicle (1.75 m below the carriage) and the carriage is plausible. We therefore expect that the values of intercept should, in reality, be close to zero for all vehicle speed at zero drift angle. There was no clear pattern in the slope data for the high speed tests at zero drift angle. The raw data for these tests was relatively noisy, and we attribute this to the structural flexibility of the yaw frame. From the data, it seems reasonable to assume that the slope b remains constant (at about -1.1×10^{-5} N/RPM²) in this range.

High Speed Turns: Although the tunnel thrusters were not intended to be used at higher speeds they may be a useful way to increase control authority. It has been shown by Ridley (1971) that bow thrusters are an effective steering aid in surface ships with headway. It is assumed that a similar effect would apply to underwater vehicles using tunnel thrusters. The detailed data for the high-speed turns is presented in Saunders (2002). That data shows that, at positive drift angles, increasing speed leads to a slight increase in the axial thrust produced for a given RPM (i.e. the magnitude of b increases with forward speed). This effect is opposite to that observed at lower speeds in the lower part of Fig. 10. For negative drift angles, the opposite is true: increasing

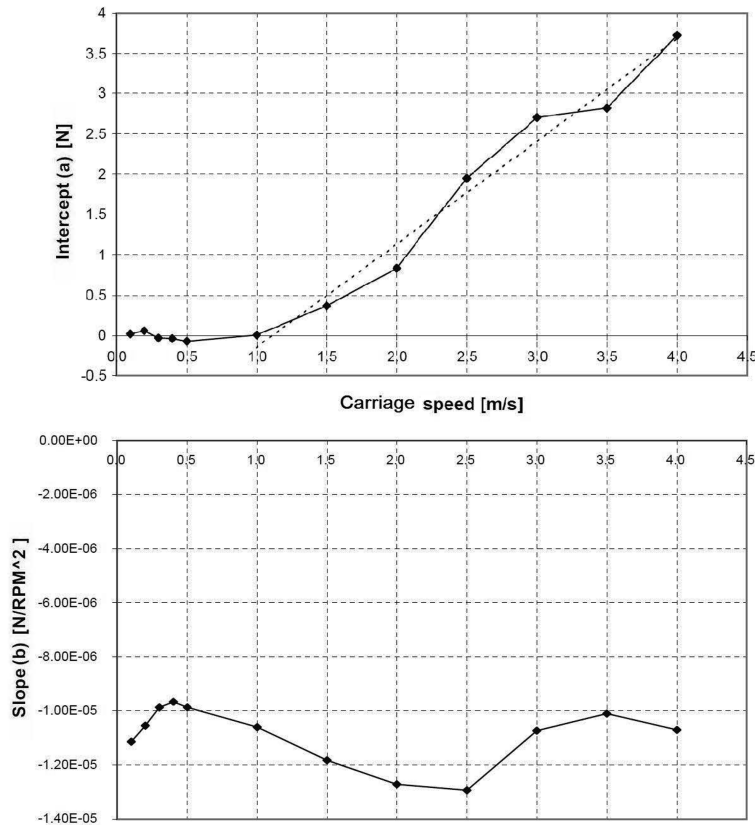


Fig. 11 Forward travel axial thrust intercept and slope values

carriage speed leads to a reduction in thrust. Additionally, the magnitude of this reduction does not seem to be constant with increasing drift angles.

3.3 Transient test results

In order to capture the thruster’s transient behavior, square wave commands in RPM were used. The same test matrix was used for the transient tests as in the steady state tests (Fig. 6). At each of these conditions the thruster was cycled through a series of alternating step inputs from forward speed to reverse speed. In general, the transient behavior did not change significantly with drift or vehicle speed. For example, Fig. 12 shows the response of the thruster for several values of carriage speed (0.1 to 0.5 m/s) at 30° yaw. The overall shape and magnitude of the different curves match closely. The only significant difference between the curves is the reduction in steady state thrust as carriage speed is increased. This issue was addressed in some detail in the previous section. The close match between transients was also observed at higher carriage speeds, and over the full range of yaw angles. From this, we can conclude that vehicle speed and orientation do not have a significant effect on transient thruster performance, and that static transient thruster tests can be used to define the transient performance of the tunnel thruster unit.

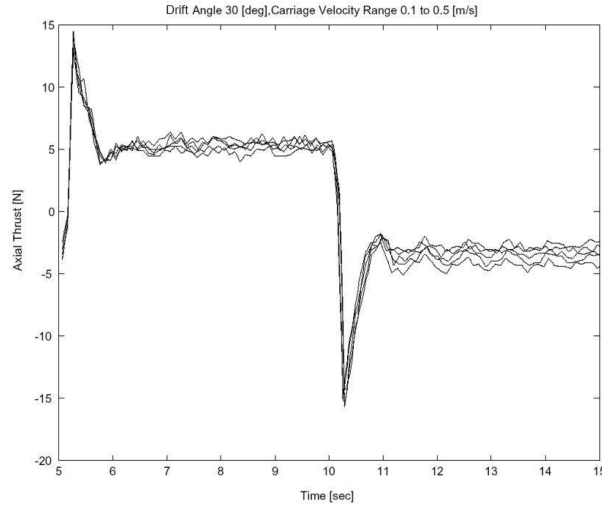


Fig. 12 Square wave response. The abscissa shows the elapsed time for a response to a square wave input with a 10 s period, beginning at $t = 5$ s.

4. Modelling

This section reviews an existing tunnel thruster model which is then adapted to include the effects of vehicle speed and orientation, based on the experimental results from Section 3.

4.1 Basic model

Our ‘basic’ model is loosely based on the work by Brown (1993) and Healey *et al.* (1995) who focused on the characterization of a *static* thruster (i.e., the ambient axial water velocity, $U_\infty = 0$). A block diagram of their model is shown in Fig. 13. The original model included two coupled nonlinear first order differential equations, and thus two state variables. Whitcomb and Yoerger (1999) showed that when the motor is equipped with an internal speed sensing loop, the model is reduced to only a single first order differential equation with a single state variable: the fluid velocity at the propeller U_a . Accordingly, since our setup uses propeller speed as the control input, the upper part of the block diagram shown in Fig. 13 was no longer needed.

The reduction in model order from two to one state variables removes the uncertainties involved in modelling the electro-mechanical system by using the speed sensor feedback from the motor. However, it relies on having a robust inner motor speed loop which can be relied on to provide the commanded propeller speed accurately and with no lag. This corresponds to our experimental setup, and leads to our ‘basic’ model governed by a single differential equation (Whitcomb and Yoerger 1999)

$$F_a = K_1 \dot{U}_a + K_2 U_a |U_a| \quad (2)$$

where $K_1 = \rho A l \gamma$ and $K_2 = \Delta \beta \rho A$. U_a is the fluid velocity at the propeller, F_a is output thrust, ρ is the water density, A and l are the duct area and length, γ is an empirically determined added mass coefficient, and $\Delta \beta$ is a momentum flux coefficient (Brown 1993). The resulting model block diagram is shown in Fig. 14. In Eq. (2), the output thrust is seen to consist of two components. The

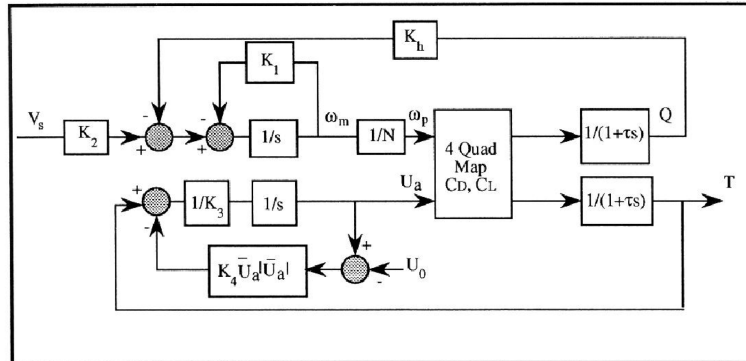


Fig. 13 Brown's (1993) system model. Note that some symbols in this diagram do not correspond to those used in this paper.

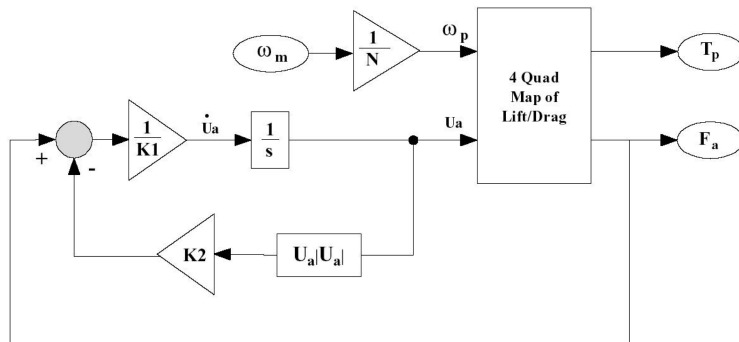


Fig. 14 The basic model

first term on the right-hand-side corresponds to the transient effects, while the second term corresponds to the steady-state thrust. It can also be shown that the second component can also be written in the form given by Eq. (1), with $a = 0$, for the case of a static thruster.

It is important to note the limitations of the models discussed above. The basic model is unable to model a thruster mounted in a vehicle moving forward with sideslip (drift). This can be traced to the fact that (a) the governing equations were developed with the assumption that the ambient water velocity is zero, and (b) the model presumes symmetry in the thruster's performance with respect to positive/negative RPM. This latter assumption is clearly flawed, as seen in the experimental data shown by Brown (1993) and Healey *et al.* (1995), and as was evident in the data shown here earlier.

4.2 Modelling the effects of vehicle speed and drift

The most significant limitation of the model presented in the previous section is its assumption of zero ambient axial water velocity. This section discusses a means for including the effects of vehicle speed and orientation into the tunnel thruster model. In order to model a thruster that is moving through the water with a vehicle, the effect of the inlet water velocity must be taken into consideration. The model presented by Blanke *et al.* (2000) included the effects of nonzero vessel speed relative to the water. That model is developed in much the same way as Brown's (1993)

model, with the exception that it does not assume a zero ambient water velocity. In this case, we find that the development leads to

$$F_a = K_1 \dot{U}_a + K_2 (U_a - U_\infty) |U_a| \quad (3)$$

where U_∞ is the ambient axial water velocity. In ship modelling, U_∞ is usually equivalent to the forward vessel speed. The addition of vessel speed will improve the accuracy of the model for a thruster whose axis is parallel to the direction of travel. However, with a through-body thruster, the thrust axis is seldom parallel to the direction of travel, and so the effect of vehicle orientation must also be taken into account.

In order to capture effects of vehicle speed and orientation, we return to the experimental results presented in Section 3. It was observed there that vehicle speed and orientation had little effect on the transient behavior of the thruster. This allows us to keep the transient portion of Eq. (2) intact and concentrate on modifying the steady state portion. It was shown that the experimental steady state results could be condensed into the relationship given by Eq. (1). By replacing the steady state portion of Eq. (2) by Eq. (1), we obtain the following first order differential equation

$$F_a = K_1 \dot{U}_a + a + b \omega_p |\omega_p| \quad (4)$$

4.3 Augmented model

The approach discussed in the preceding section allows us to capture the effects of vehicle speed and drift angle in an ‘Augmented Model’. The key differences between the basic and augmented models are as follows:

- The effects of forward vehicle speed and orientation are included by using the experimental results from tow tank testing. This is achieved through the use of lookup tables for a and b over the entire range of vehicle speeds and drift angles tested in this work.
- The effects of asymmetry in transient thruster performance are captured by tuning γ separately for the forward and reverse axial flow case. In the simulation, the direction of axial water flow, U_a , is evaluated at each pass through and the appropriate forward or reverse γ is used.

Non zero values of a are due to the forces in the thruster unit for $\omega_p = 0$. As shown in the upper part of Fig. 10, a is a function of drift angle and vehicle speed. The value of b is a function of drift angle, vehicle speed, and the direction of U_a . In particular, we must account for the direction of U_a relative to a particular vehicle speed and drift angle, as shown in Fig. 8. The tow tank tests were run for drift angles in the range of $\pm 90^\circ$, but always for positive ω_p ramps. Therefore, the values of b available are for one direction of U_a corresponding to a particular drift angle and vehicle speed. We presume that the value of the slope b for negative ω_p at a particular speed and drift angle is the same as for positive ω_p at the same speed but the negative drift angle. In addition to this, the value of b must be modified if ω_p is in the negative direction to account for the asymmetry in steady state thrust, shown in Fig. 7. This is done by multiplying b by a modifier, b_{Mod} , which corresponds to the increase in the slope of b observed in the steady state tests for negative ω_p . The resulting model is shown in Fig. 15.

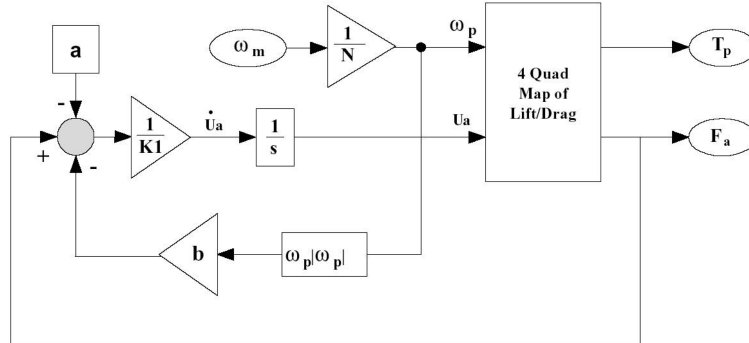


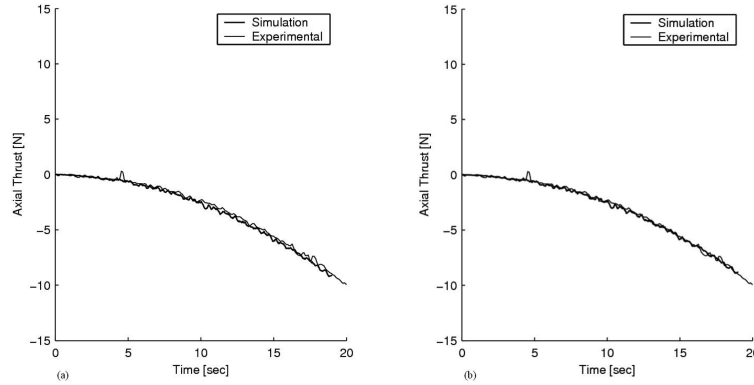
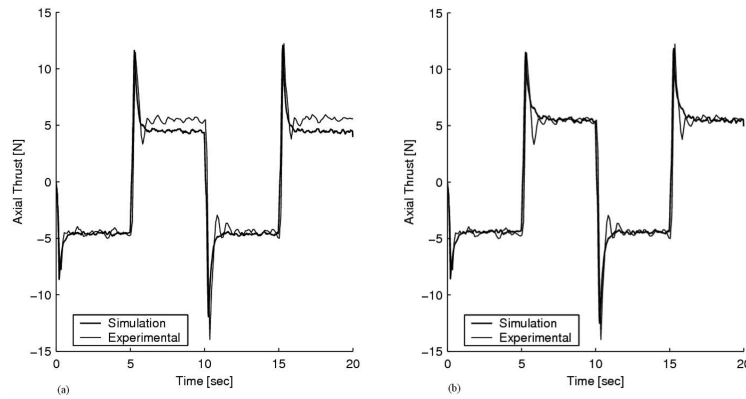
Fig. 15 The augmented model

4.4 Simulation results

We are now in a position to compare the capabilities of the basic and augmented models. It is important to note the method of identification for different model parameters. In the basic simulation, there are four parameters that must be manually selected: γ , the added mass coefficient; $\Delta\beta$, the momentum flux coefficient; C_{Lmax} , the maximum lift coefficient; and C_{Dmax} , the maximum drag coefficient. This is referred to as ‘tuning the model’---a process by which the model parameters are varied until the simulation output matches an experimental data set. In general, the axial force transient peak was matched by adjusting γ and C_{Lmax} , the steady state thrust by adjusting $\Delta\beta$ and C_{Lmax} , and finally the propeller hydrodynamic torque load by adjusting C_{Dmax} . Because the parameters cannot be tuned independently, their final values are somewhat arbitrary. However, it is important to ensure that the values stay within their physically meaningful range. For example, $\Delta\beta$ cannot exceed 2 (its ideal value, predicted by momentum theory); for low aspect ratio wing section, C_{Lmax} rarely exceeds 1.0; and the flat plate drag C_{Dmax} will generally not exceed 2. With these ranges defined, the basic model was manually tuned and the resulting parameter values are presented in Table 1. For the present purpose, the model was tuned to match the forward steady state thrust as closely as possible.

Table 1 Basic model parameters

Parameter	Value	Units	ID method
D	0.1016	m	measured
l	0.410	m	measured
A	0.00811	m ²	measured
γ	1.2	--	Tuned
$\Delta\beta$	1.7	--	Tuned
ρ	998	kg/m ³	handbook
C_{Lmax}	0.6	--	Tuned
C_{Dmax}	1.125	--	Tuned
ϕ	0.4268	rad	measured

Fig. 16 Slow ramp response, $V = 0.1$ m/s, Drift = 0Fig. 17 Square wave response, $V = 0.1$ m/s, Drift = 0

Figs. 16(a) and 17(a) show the response to a slow positive ramp input and to a square wave input in ω_p , respectively, for $V = 0.1$ m/s and Drift = 0. Under these conditions, the basic model does a reasonable job of matching the experimental data, though it does miss the asymmetry in steady-state performance (positive plateaus in Fig. 17(a)). This observation, in addition to the transient tow tank results, supports the idea that only the steady state portion of the model needs to be replaced. Under more extreme conditions of $V = 0.5$ m/s and Drift = 90° , shown in Figs. 18(a) and 19(a), the basic model's performance is much less satisfactory. Both Figs. 18(a) and 19(a) show a significant mismatch in steady state and transient thrust between the basic model and experimental data.

We now turn our attention to the augmented model. For this simulation there are only three tuned parameters: γ , C_{Lmax} and C_{Dmax} . Because the propeller geometry has not changed, there is no justification for changing the value of C_{Lmax} or C_{Dmax} from the basic model. This leaves only one variable to tune: γ , which will have a different value for forward and reverse axial flow directions.

In general, an increase in γ results in an increase in thrust overshoot and settling time. Values for forward and reverse γ were obtained by tuning the model for the stationary thruster case. The new additions to the model are the experimentally fitted values of intercept and slope, a and b , from Fig. 10. These values were integrated into the simulation using lookup tables. Overall, the augmented model requires less tuning due to the addition of the lookup tables. The resulting parameter values for the

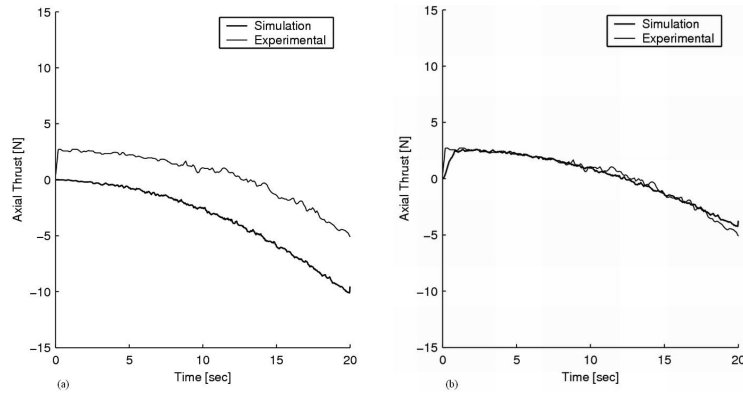


Fig. 18. Slow ramp response, $V = 0.5$ m/s, Drift = 90°

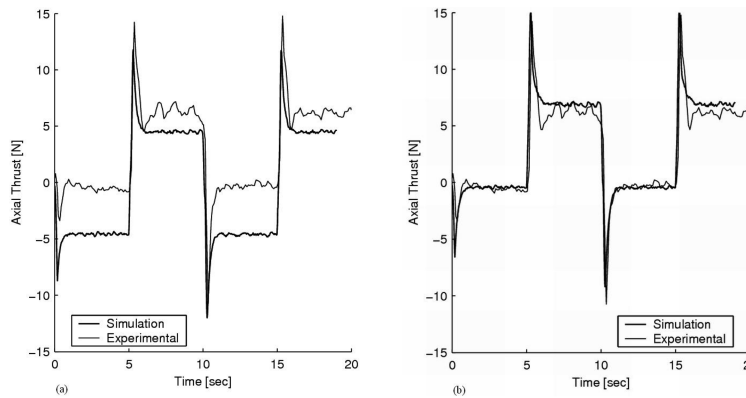


Fig. 19. Square wave response, $V = 0.5$ m/s, Drift = 90°

augmented simulation are presented in Table 2.

In order to demonstrate the capabilities of the augmented model, the same test cases are considered as for the basic model. Figs. 16(b) and 17(b) show the response to a slow positive ramp input and to a square wave input in ω_p , respectively, for $V = 0.1$ m/s and Drift = 0. Here, the results from the augmented model match the experimental data quite well, including the asymmetry in steady-state performance (positive plateaus in Fig. 17(b)). For the more extreme conditions of $V = 0.5$ m/s and Drift = 90° , shown in Figs. 18(b) and 19(b), the augmented model's performance is again very good. This was true, in general, for all conditions, the exceptions being at large drift angles and speeds above 0.4 m/s. Fig. 19(b) shows that the settling time of the predicted thrust overshoot does not match the experimental data at these conditions. This mismatch at large drift angles is most likely due to the error in fitting the a 's and b 's to the experimental thruster data by the large amount of scatter for these more extreme test cases. The model was, however, able to capture the asymmetry in transient behavior very well.

In summary, the results from the augmented simulation are well within acceptable limits for representing the performance of the tunnel thruster operating in a vehicle with speed and drift. The small mismatches in modelled performance would most likely have little or no effect on the vehicle's overall operation.

Table 2 Augmented model parameters

Parameter	Value	Units	ID method
D	0.1016	m	measured
L	0.410	m	measured
A	0.00811	m ²	measured
γ_F	0.6	--	tuned
γ_R	0.9	--	tuned
ρ	998	kg/m ³	handbook
C_{Lmax}	0.6	--	tuned
C_{Dmax}	1.125	--	tuned
ϕ	0.4268	rad	measured
a	lookup	N	measured
b	lookup	N/(rad/s) ²	measured
b_{Mod}	1.267	--	measured

5. Conclusions

A small tunnel thruster was constructed, mounted in an AUV and tested in a tow tank at various carriage speeds and drift angles. Overall, the tow tank testing revealed that the effects of drift and vehicle speed are fairly complex, suggesting that complicated fluid dynamics effects dominate steady state thruster performance. The linear relationship between axial thrust and propeller rotational speed squared was found to hold for the full range of conditions. The steady state tests revealed that (a) thruster performance during low speed maneuvering is only slightly reduced by vehicle speed, and that this decrease in steady state thrust becomes more pronounced as the drift angle is increased; (b) there exists a definite asymmetry in thruster performance with respect to positive/negative drift angles; and (c) there exists a distinct asymmetry in thruster performance with respect to positive/negative RPM. The transient test results were relatively unaffected by vehicle speed and drift angles, but there existed a distinct asymmetry in response with respect to positive/negative RPM.

It was shown that existing tunnel thruster models do not capture asymmetry in axial thrust performance, and definitely cannot model the effects of vehicle speed and drift angle. A new tunnel thruster model was assembled, loosely based on existing thruster models. Because the transient behavior did not change significantly with drift angle and vehicle speed, only the steady state portion of the thruster model needed to be modified. The coefficients a and b , extracted from the experimental data were used directly to replace the steady state part of the tunnel thruster model. Asymmetry in transient behavior was handled by separately tuning the added mass coefficient for the forward and reverse axial flow conditions. The new model was successful in capturing the effects of vehicle speed and drift as well as asymmetry in thruster performance.

Acknowledgements

The authors gratefully acknowledge the financial support of the Natural Sciences and Engineering Research Council for this work. As well, we wish to thank Chris Williams and Tony Randell at the NRC Institute for Ocean Technology and Neil Bose and Jim Gauss of MUN for their help in the use of IOT and MUN facilities.

References

- Bachmayer, R., Whitcomb, M. and Grosenbaugh, M. (1998), "A four quadrant finite dimensional thruster model", *Proceedings of the OCEANS'98 IEEE Conference*, Nice, France.
- Bachmayer, R., Yoerger, D. and Grosenbaugh, M. (2000), "An accurate four-quadrant nonlinear dynamical model for marine thrusters: theory and experimental validation", *IEEE J. Oceanic Eng.*, **25**(1), 146–159.
- Beveridge, J. (1972), "Design and performance of bow thrusters", *Mar. Technol. Soc. J.*, **9**(4), 439–453.
- Blanke, M., Linaard, K. and Fossen, T. (2000), "Dynamic model for thrust generation of marine propellers", *Proceedings of the Conference on Marine Craft Maneuvering and Control*.
- Brown, J. (1993), *Four quadrant dynamical model of the AUV II thruster*, Master's thesis, Naval Postgraduate School, Monterey, California.
- Curtis, T., Perrault, D., Williams, C. and Bose, N. (2000), "C-SCOUT: a general-purpose AUV for systems research", Presented at Underwater Technology.
- Evans, J. and Nahon, M. (2004), "Dynamics modeling and performance evaluation of an autonomous underwater vehicle", *Ocean Eng.*, **31**(14-15), 1835-1858.
- Healey, A., Rock, S., Cody, S. and Brown, J. (1995), "Toward an improved understanding of thruster dynamics for underwater vehicles", *IEEE J. Oceanic Eng.*, **20**(4), 354–361.
- Kim, J. and Chung, W.K. (2006), "Accurate and practical thruster modeling for underwater vehicles", *Ocean Eng.*, **33**(5-6), 566-586.
- Mailfert, G. and LeMaire, J. (1998), "REDERMOR: an experimental platform for ROV/AUV field sea trial", *Proceedings of the OCEANS'98 IEEE Conference*, Nice, France.
- Marco, D. and Healey, A. (2000), "Current developments in underwater vehicle control and navigation: The NPS ARIES AUV", *Proceedings of the OCEAN 2000 MTS/IEEE Conference*, Providence, RI.
- McLean, M. (1991), *Dynamical performance of small diameter tunnel thrusters*, Master's Thesis, Naval Postgraduate School, Monterey, California.
- Palmer, A., Hearn, G.E. and Stevenson, P. (2008), "Modelling tunnel thrusters for autonomous underwater vehicles", *Proceedings of the navigation, guidance and control of underwater vehicles, International Federation of Automatic Control (IFAC)*, Killaloe, Ireland.
- Ridley, D. (1971), "Observations on the effect of vessel speed on bow thruster performance", *Mar. Technol. Soc. J.*, **8**(1), 93–96.
- Saunders, A. (2002), *The effect of velocity and orientation on the simulation and experimental characterization of an AUV tunnel thruster*, M.A.Sc. Thesis, University of Victoria.
- Whitcomb, L. and Yoerger, D. (1999), "Development, comparison, and preliminary experimental validation of non-linear dynamic thruster models", *IEEE J. Oceanic Eng.*, **24**(4), 495–506.
- Whitney, J. and Smith, S. (1998), "Observations on the dynamic performance of tunnel thrusters", *Proceedings of the OCEANS'98 IEEE Conference*, Nice, France.
- Yoerger, D., Cooke, J. and Slotine, J. (1990), "The influence of thruster dynamics on underwater vehicle behavior and their incorporation into control system design", *IEEE J. Oceanic Eng.*, **15**(3), 167–178.